Simulation and Design Considerations of a Dual Layer Plastic Scintillator Intra-Operative Probe for Radiolabelled Tumours

Martin A. Belzunce, Samuela Lomazzi, Monica Beretta, Massimo Caccia and Andrew J. Reader

***Abstract*—The design of intra-operative hand-held imaging devices that assist surgeons with the complete removal of radioactively labelled tumours is an important problem to solve in cancer surgery. A number of different designs for such devices have been proposed previously but they have not been completely successful in providing real-time images due to the difficulty in discriminating the background from the tumour radiation. Recently, a novel approach that uses two layers of ultrathin detector foils to measure the direction of the detected positrons was proposed at Arizona University. This new concept, called a directional charged particle detector, is able to detect the direction of the detected particles by measuring the position of interaction of the positron in each detection layer. Despite having a clear working principle, there are a number of issues to be addressed in the implementation of this concept in an intra-operative probe. In this work, we perform a simulation study to characterize and optimize a probe design that uses two thin plastic scintillators as detector layers and a silicon photomultiplier as a photo-detector. The impact of the scintillator thickness on the spatial resolution and sensitivity of the probe was evaluated using Monte Carlo simulations. Taking into account only the positron physics and a probe-tumour distance of 10 mm, the probe intrinsic spatial resolution was in the range of 3.5-7.5 mm. If a cover foil is added to protect the probe, the resolution is degraded to 7-10 mm. The tumour-gamma background discrimination was studied by simulating a gamma background source coming from the patient's body, and it was found to be negligible due to the thin plastic scintillators and the use of coincidence events. The design was further evaluated including the generation and transport of the optical photons, as well as the photo-detector readout. A scintillator thickness between 25 and 50 $\mu\mathrm{m}$ with a separation between the two layers of 1000 $\mu\mathrm{m}$ proved to be a good compromise regarding spatial resolution and sensitivity. With this parameter choice and without the foil cover, the intra-operative probe could reconstruct a point source with a FWHM of 10 mm, that can be improved to 5 mm when reconstructing the images via iterative methods. According to our study, the reduction of the thickness of the foil cover, the introduction of new and better plastic scintillators and the current advances in silicon photomulpliers are key points to improve the limited spatial resolution achievable with a dual layer intra-operative probe.**

***Index Terms*—Intra-operative probe, Positron, Direction Charged Patricle Detector, Monte Carlo Simulations, Image Reconstruction, Cancer Surgery.**

I. Introduction

ADVANCES in medical imaging, especially in positron emission tomography (PET), have dramatically helped to improve cancer diagnosis. However, diagnostic images obtained during the screening process are inadequate to assist surgeons during cancer surgery, which remains the first treatment option for most types of cancer. As a consequence, cancer surgeries has a significant failure rate due to incomplete removal of the tumour. The outcomes of failed surgery can include repeat operations, higher risk of recurrence, more extensive post-surgical treatment, and lower survival rates. For example, one in five patients undergoing surgery for early-stage breast cancer will require a further operation due to the incomplete surgical removal of the cancer in the first operation [1].

Surgeons today rely on doing biopsies during surgery to check for the need of removal of additional tissue and also on post-surgical pathology tests, which can take several days, to assess whether cancer has been left behind. Therefore, intra-operative diagnostic imaging is an important problem to solve in cancer surgery that could bring significant benefits to both the patient and healthcare systems. Using a PET scanner routinely in a operation room is not feasible because of its size and high cost. Consequently, there is a need to design and develop intra-operative hand-held devices to be used in conjunction with a radiotracer. A number of different designs for such devices have been proposed previously and they can be divided into two main categories: beta particle detection devices [2]–[8] and gamma detection devices [9]–[11]. However, most of these probes do not have imaging capabilities and, as a consequence, cannot provide information about the boundaries of the tumour to be removed.

The intra-operative probes that are able to provide images have not been completely successful in providing real-time images for cancer detection during surgery because of the difficulty of discriminating the background from the tumour radiation. The latter is an extremely challenging problem due to the large background activity that comes from the healthy tissue surrounding the cancerous tissue and from organs with high radiotracer uptake, such as the bladder or the heart. Imaging probes can be based on the detection of gamma photons or beta particles as both are correlated, although beta detections may offer superior real-time localization of tumour deposits [12]. Most of the probes that use gamma radiation cannot selectively enhance the sensitivity to the tumour radiation. However, if the probe is sensitive to the positrons emitted from the tumour, that do not annihilate because they are near the surface tissue during the surgery, the detector can be optimized to be more sensitive to beta particles than to 511 keV gamma photons. In this sense, probes that use thin plastic scintillators or phosphor plates have been proposed with an improvement in the gamma-tumour discrimination [7], [13].

The current design of beta imaging probes generate planar images as they cannot measure the direction of the incident particles [4], [7], [14], [15]. Therefore, they suffer from an exponential degradation of the spatial resolution when the probe is moved away from the patient to a reasonable distance that would avoid contact with tissue and

Martin A. Belzunce and Andrew J. Reader are with King's College London, School of Biomedical Engineering and Imaging Sciences, St Thomas's Hospital, London, UK. Samuela Lomazzi Monica Beretta and Massimo Caccia are with Università dell'Insubria, Dipartimento di Scienza ed Alta Tecnologia, Como, Italy.

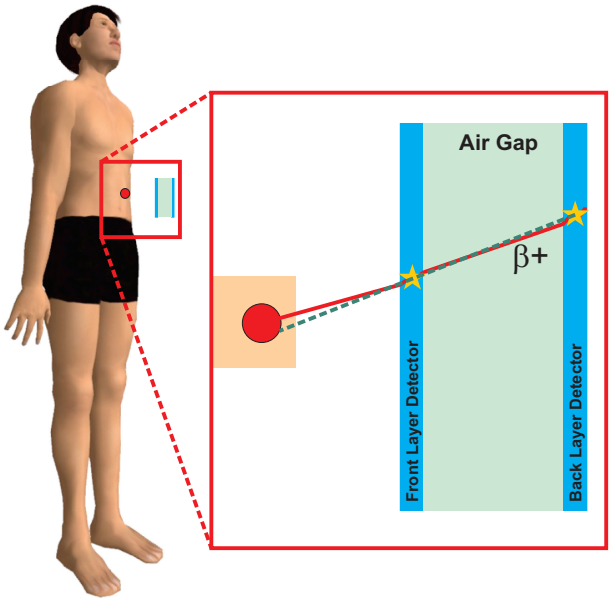

Fig. 1. Basic principle of an intra-operative probe based on a directional charged-particle detector. The probe is positioned close to the superficial tumour to be assessed. The positrons escaping from the patient's body are first detected by a front layer detector, which only takes a small amount of energy from the charged particle, and then in a back layer detector, both separated by an air gap. With the estimation of the impact point in each layer, the direction of the positron can be calculated and then backprojected into the imaging plane.

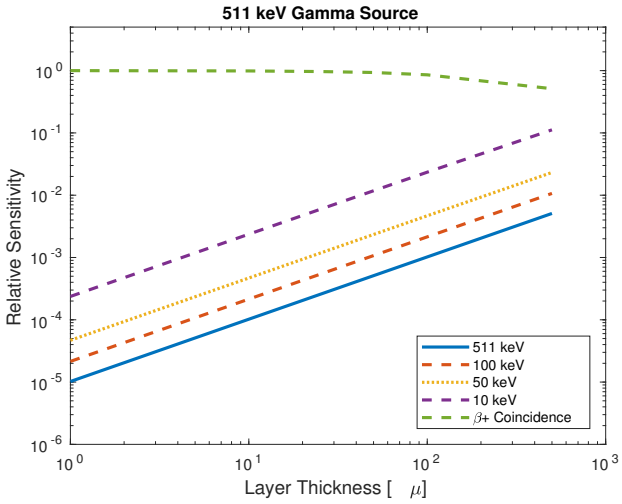

Fig. 2. Theoretical count rates in a plastic scintillator for collimated gamma sources of 511, 100, 50 and 10 keV and the coincidence count rate in a dual layer probe for a collimated $\beta+$ source (^{18}F), both as a function of the scintillator thickness.

the contamination of the probe. To be able to enhance the imaging capabilities it is necessary to be able to detect the direction of the detected particles. The use of a collimator can help to detect particles that arrive at the detector in known directions, however this brings a significant loss of sensitivity which it is not tolerable for this kind of application.

Recently, a novel approach that uses two layers of ultrathin phosphor foils to measure the direction of the detected positrons was proposed by Barrett et al at the University of Arizona [16], [17]. This new concept, called a directional charged particle detector (DCPD) is based on measuring the position of interaction of the positron in each detection layer to estimate the line of response (LOR) as depicted in Fig. 1. To achieve this, each foil needs to be extremely thin in order to avoid a large change of the particle direction due to multiple Coulomb scattering in the detector. On the other hand, each layer needs to be thick enough to generate a sufficient number of optical photons in order to estimate the interaction positions.

Moreover, the use of thin detector layers makes the probe more immune to the gamma background originating from the annihilation of the radiotracer positrons distributed in the patient's body and therefore being several orders of magnitude greater in intensity than the positrons coming from the tumour surface. In Fig. 2, we compare the detection sensitivity of a generic plastic scintillator exposed to a collimated gamma point source (computed using the mass attenuation coefficient (μ/ρ) [18]) to the sensitivity of a dual layer probe exposed to a collimated $\beta+$ point source with the same activity (obtained with Monte Carlo simulations). For the latter, we considered the sensitivity to coincidence events (i.e. a detected event is counted only if the positron deposited energy in both layers). The sensitivity values are relative to the sensitivity of a dual layer probe with 1 μm thick scintillators. We can see that the probe is more sensitive to the low energy photons ($\sim$ 10 keV) than to the 511 keV photons by more than one order of magnitude. For this reason, to assess the behaviour of the probe in real conditions it is important to simulate accurately the gamma background including the scattered photons in the patient's body.

In this work, we perform a simulation study to characterize and improve the design of an intra-operative probe based on the DCPD concept presented in [16], [17]. In the proposed design, we used two thin plastic scintillators as detectors instead of the phosphor foils used in the aforementioned work. Firstly, we identified the main factors that affect the feasibility of this kind of probe and then evaluated the impact of a set of design parameters on the spatial resolution and sensitivity of the probe using Monte Carlo simulations. The latter were carried out using GATE [19] and included a realistic tumour activity concentration and the gamma background coming from the patient's body. Monte Carlo simulations that take into account only the positron physics were used to estimate the deviation of the positrons in each detection layer. Additionally, the design was further evaluated including in the simulations the generation and transport of the optical photons, as well as the photo-detector readout. The simulations were validated using a simple experimental setup. Finally, the impact of an iterative reconstruction algorithm on the reconstructed images was also assessed.

II. Materials and Methods

The simulation study performed in this work assess the feasibility of using the novel DCPD concept in a charged particle intra-operative probe, which should be capable of doing real-time diagnostic imaging during cancer surgery where the patient has been previously injected with a radiopharmaceutical, typically [^{18}F]fluorodeoxyglucose (FDG). Ideally, the probe should be able to achieve a spatial resolution better than 5 mm and to improve the specificity of beta particles over gamma particles. Each detection layer needs to be as thin as possible in order to reduce the particle scattering in the detector, which is considerable even for travel distances of the order of microns; and, on the other hand, to be thick

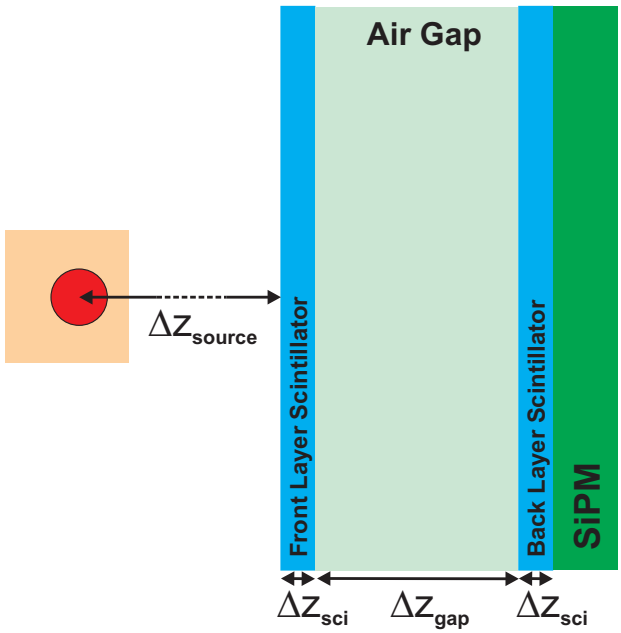

Fig. 3. Basic configuration and parameters used in the simulation of the proposed dual layer intra-operative probe. A source is located at a distance of ΔZ_{source} from the front layer of the probe. Both the front and back layer scintillators have a thickness of ΔZ_{sci} and they are separated by an air gap of ΔZ_{gap}. On the back of the back layer, a silicon photomultiplier is used to detect the optical photons.

enough to generate a signal that can be processed by the readout electronics in order to detect the particle and estimate the impact point.

In [17], the DCPD proposed implementation has two ultrathin phosphor foils, each of them consisting of a 3.5 µm thick layer of P43 phosphor powder coated on a 3 µm thick clear Mylar, an air gap separation of 125 µm and a readout based on an image intensifier and a CCD camera. In our design, we use two layers of plastic scintillators and a readout based on a silicon photomultiplier (SiPM) (shown in Fig. 3) in order to simplify the system and make it cost effective and compliant with the requirement of having a hand-held instrument. We call the detection layer closest to the source the front layer, and we call the detection layer closest to the SiPM the back layer. The photon sensor has to comply with two functionalities:

- Separate the signals by the layer where they were originated (i.e. front and back layers), for instance considering scintillators with different decay times.
- Estimate the particle impact point by reconstructing the profile of the scintillation photons using pixelated photo-detectors.

Presuming the first functionality to be implemented with a technically viable solution, the simulations carried out in this work aim to evaluate the achievable system performance in the working conditions of an operation room.

A. Design of a Dual Thin Layer Intra-Operative Probe

The objective of a dual thin layer intra-operative probe is to generate an image of the radiotracer distribution on the surface of the patient. The image is reconstructed from a list of coincidence events where the positron was detected by the two layers. The detection positions in the front and back layers are needed to form an LOR and a set of LORs can be used to reconstruct a 3D image of the distribution of the radiotracer. The detection positions, which we call (x_{1d}, y_{1d}, z_{1d}) for the front layer and (x_{2d}, y_{2d}, z_{2d}) for the back layer, are estimated by the analysis of the profile of the detected scintillation light. Because of the short positron range in tissue, this image will be mainly superficial and therefore a 2D image is reconstructed for a given plane on the tissue surface of the patient's body. Consequently, each LOR can be backprojected into a plane located at ΔZ_{source} from the front layer with the following equations:

$$x_{0\_bp} = x_{1d} + \frac{x_{1d} - x_{2d}}{\Delta Z_{gap} + \Delta Z_{sci}} \cdot \Delta Z_{source} \tag{1}$$

$$y_{0\_bp} = y_{1d} + \frac{y_{1d} - y_{2d}}{\Delta Z_{gap} + \Delta Z_{sci}} \cdot \Delta Z_{source} \tag{2}$$

where x_{0_bp} and y_{0_bp} are the coordinates of the backprojected point, ΔZ_{source} is the distance from the reconstruction plane to the front layer and ΔZ_{gap} is the separation between the two layers as depicted in Fig. 3. For z_{1d} and z_{2d}, the axial centres of each scintillator were used, therefore the distance in the z direction between the two detection positions is $\Delta Z_{gap} + \Delta Z_{sci}$.

The resolution of the system is limited by the positron physics, the geometry of the probe and the optical readout of the detector. Each of this factors will impact on the point spread function (PSF) of the system in different ways:

- The multiple scattering in the front layer deviates the positron and, as a consequence, the estimated LOR between the two interaction positions has a different direction to the original trajectory of the positron, even for perfect estimation of the impact position on each layer.
- The resolution of the estimation of the impact point on the front and back layer has a direct impact on the reconstruction of the particle trajectory after interacting in the first layer. The resolution in each layer depends primarily on the number of detected photons, their spatial distribution on the SiPM surface and the granularity of the SiPM.
- The system geometry has a considerable impact on the resolution of the backprojected point, since the uncertainty of the impact position in each layer is amplified by the ratio $\Delta Z_{source}/(\Delta Z_{gap} + \Delta Z_{sci})$.

In Fig. 4 we can observe graphically the factors that introduce errors in the estimation of the emission position of the positron. The uncertainty in the estimation of the backprojected coordinates (equations 1 and 2) can be computed by propagating the uncertainty of the estimated impact point in the first and second layer:

$$\sigma_{x_{0\_bp}} = \sqrt{\left(\frac{\partial x_{0\_bp}}{\partial x_{1d}}\sigma_{x_{1d}}\right)^2 + \left(\frac{\partial x_{0\_bp}}{\partial x_{2d}}\sigma_{x_{2d}}\right)^2}$$
$$\sigma_{x_{0\_bp}} = \sqrt{(1+n)^2\,\sigma_{x_{1d}}^2 + n^2\sigma_{x_{2d}}^2} \tag{3}$$

with

$$n = \frac{\Delta Z_{source}}{\Delta Z_{gap} + \Delta Z_{sci}} \tag{4}$$

Since $n >> 1$, the uncertainty in the estimation of the impact points for the front and back layer impacts similarly on the uncertainty of the backprojected point, where the resolution in both layers is worsened by a factor of n. Considering that the detection layers are expected to be extremely thin, in most of

the configurations ΔZ_{sci} can be considered negligible compared to ΔZ_{gap} ($\Delta Z_{gap} >> \Delta Z_{sci}$) and for those cases n can be approximated by $\Delta Z_{source}/\Delta Z_{gap}$.

Equation (3) does not account for the error added by the deviation of the positron in the first layer, which is intrinsic to this kind of probe. Therefore, the total error in the backprojected point is the sum in quadrature of the error due to the uncertainty in the estimation of the LOR and the error due to the change of direction of the positron after interacting with the front layer. The latter depends on the angle of incidence (α) of the particle, the mean deviation angle (θ) of the positron after interacting with the front layer and on the distance from the source to the front layer:

$$\sigma_\theta = \Delta Z_{source} \cdot [\tan(\alpha + \theta) - \tan(\alpha - \theta)] \quad (5)$$

where σ_θ is the total error but is asymmetric with respect to the emission coordinate $\Delta Z_{source} \tan(\alpha)$. For a particle travelling perpendicular to the probe ($\alpha = 0$) as in Fig. 4, the error is symmetric and equation (5) can be simplified to:

$$\sigma_\theta = 2\Delta Z_{source} \cdot \tan(\theta) \quad (6)$$

Therefore, the total uncertainty in the estimation of the emission position of the positron (σ_{x_0}) is the sum in quadrature of equations (3) and (6):

$$\sigma_{x_0} = \sqrt{(1+n)^2\sigma_{x_{1d}}^2 + n^2\sigma_{x_{2d}}^2 + (2\Delta Z_{source} \cdot \tan\theta)^2} \quad (7)$$

It can be seen that for $n >> 1$ the uncertainty σ_{x_0} depends linearly on the distance to the source and that the first two terms can be potentially reduced by increasing the distance between layers (ΔZ_{gap}). For that reason the impact of the detector spatial resolution on the resolution of the reconstructed images needs to be assessed along with the separation between the layers (air gap). The readout electronics and the number of optical photons generated in each scintillator will determine the spatial resolution on the detector.

The photon sensor has the additional task of layer identification that will not be considered in this work. However, it is expected that there will always be crosstalk between the signals generated from the front and back layers. The latter implies that photoelectrons generated in one layer will be used to estimate the impact point on the other layer, which will degrade the spatial resolution of the estimated impact points ($\sigma_{x_{1d}}$ and $\sigma_{x_{2d}}$) and consequently the system spatial resolution. In this work we will focus on the spatial resolution of the detector considering a perfect layer identification.

The mean deviation due to the multiple scattering in the front layer is an intrinsic physical limitation of a dual thin layer probe and it depends on the thickness of the first layer. This parameter will be studied in the next section with a set of simplified Monte Carlo simulations.

B. Essential Features of Positron Detection in the DCPD Probe

Arguably, the thickness of the front layer, nearest to the source, is the key parameter of the system. A thicker layer causes resolution losses and a reduction in the sensitivity due to the multiple scattering of the charged particle in the scintillator. Conversely, a thicker layer also results in greater net energy deposition per detection, which will be important for optical photon generation, and that will result in a better estimation of the position of interaction.

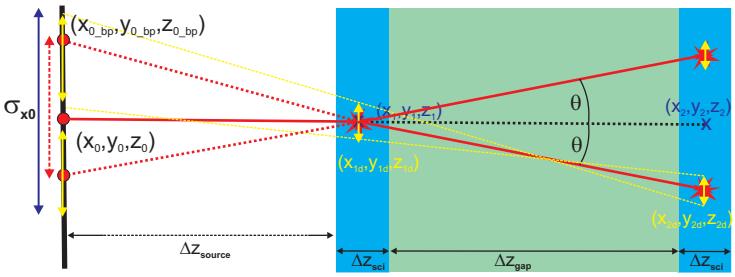

Fig. 4. Source of errors in the backprojection of a detected event in a dual layer probe. In red the deviated positron trajectory is shown. In dashed red the error due to the angular deviation of the positron after interacting with the first layer, in yellow the error due to the uncertainty in the impact position on each layer and in dark blue the total error (σ_{x_0}) for the backprojected event.

We estimated the positron angular deviation in the first layer, as well as other parameters, as a function of the scintillator thickness by running Monte Carlo simulations. These simulations were used to characterize the behaviour of the probe only for the positron physics so as to study the limits of this type of detector, therefore the generation of optical photons and the detector readout were not included in this first set of simulations. We simulated with GATE the geometry presented in Fig. 3 with an ^{18}F point source located at 10 mm from the front layer scintillator (ΔZ_{source}) and with a separation between layers (ΔZ_{gap}) of 300 µm. Both layers consisted of a generic plastic scintillator of 1.032 g cm^{-3} density with side lengths of 32 mm and thicknesses (ΔZ_{sci}) of 2, 5, 10, 20, 50, 100 and 250 µm. Each positron that deposited energy in the scintillator was considered as detected (*single* events) and when a positron deposited energy in both layers we tagged it as a coincidence event. The energy distribution of the ^{18}F positrons was considered in the simulated source by using the predefined positron energy spectrum available in GATE. The energy cuts were set to 10 nm in all the simulations in order to be able to track accurately the positron in the ultra thin layers.

In Fig. 5, the main metrics obtained from this set of simulations are plotted as a function of the scintillator thickness. In a), the event rate is constant for the front layer but a decrease of the detection rates in the back layer and, as a consequence, in the coincidence events is observed for thicker scintillators caused by the deviation or absorption of the positrons in the front layer. The mean energy deposited for every detected positron in each layer is plotted in b) where, as expected, more energy is deposited for thicker layers. In c) the mean deviation after the positron went through the front layer is shown for single events. The deviation angle is computed as the angle between the vector specifying the incident direction of the positron and the vector formed by the position of the last interaction in the front layer and the first interaction in the back layer. In d) a histogram with the distribution of angle deviations for each thickness is shown.

C. Essential Features of the DCPD Probe under Realistic Working Conditions

With the objective of characterizing the physical limits of the dual layer probe in a realistic scenario for an intra-operative probe, we simulated a 1 minute probe scan of a tumour where the probe is located at 10 mm from the patient's body and where the patient's body emits a gamma background. Additionally, the

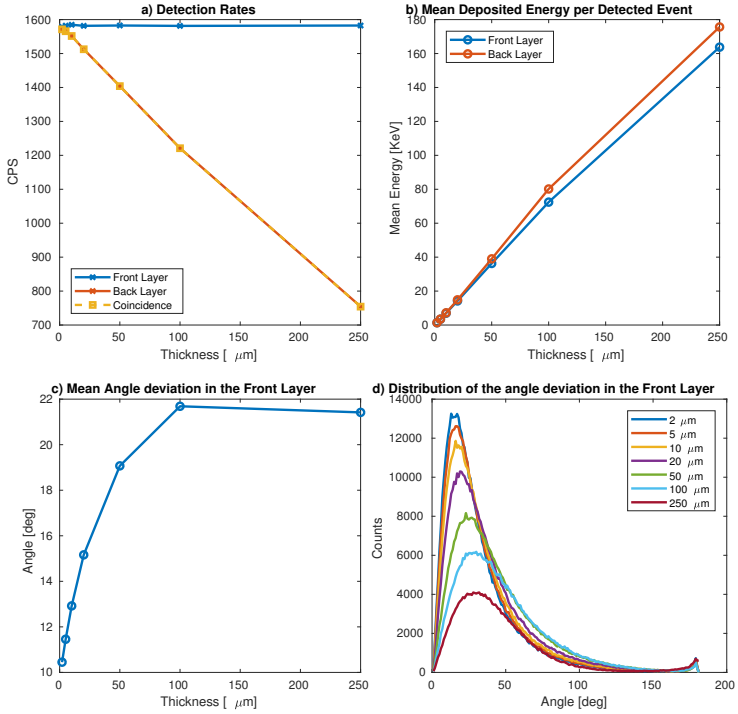

Fig. 5. Impact of the scintillator thickness on the detection properties of the probe taking into account only the physics of the charged particles. a) Detection rate in the first and second layer, and the coincidence detection rate, as a function of the scintillator thickness. b) Mean deposited energy in each layer for single events as a function of the scintillator thickness. c) Mean angle deviation of the particle after passing through the first layer for every detected positron in that layer as a function of the scintillator thickness. d) Angle deviation histograms for each scintillator thickness.

probe has a front cover foil to protect the front layer from any damage or contamination. In these simulations we considered only the physics of the charged particles without taking into consideration the imperfections of the detector, in order to asses the limitations of the probe for even a perfect readout. For each simulation, we recorded the *hits* (every single interaction in the detectors) and the *singles* (the net energy and spatial centroid of all the interactions between the particle and the detector layer). A post-processing was applied to filter each hit and single event by layer. It is important to clarify that here the detector is ideal and therefore is able to have perfect spatial resolution and every energy deposition is detected even for very low energy interactions.

The gamma source that simulates the background radiation coming from the patient's body was designed assuming that a patient of 70 kg was injected with a dose of 5 $\mathrm{MBq\,kg^{-1}}$, meaning an activity concentration of 5 $\mathrm{kBq\,cm^{-3}}$ for a body density of approximately 1 $\mathrm{g\,cm^{-3}}$. To simplify the shape of the phantom we used a cubic phantom of $170 \times 30 \times 14$ $\mathrm{cm^3}$ made of tissue with a uniformly distributed activity of 360 MBq that matches the assumed patient's volume and dose. For the lesion, a cylindrical $^{18}\mathrm{F}$ source with 2 mm radius and 0.2 mm height, with a total activity of 17 kBq was embedded in the phantom at 0.1 mm from the surface and located at 10 mm from the probe. The full width at half maximum (FWHM) of the backprojected point sources was used to measure the intrinsic resolution of the system for the described working conditions.

For the probe cover, a commercially available foil was used in the simulations and consisted of five layers: 12 μm of polyester, 3 μm of adhesive, 9 μm of aluminium, 3 μm of adhesive and 50 μm of polyethylene. The cover thickness is comparable to or even greater than the scintillator thickness, generating a larger angular deviation of the positron. For this reason, it is very important to include it in the simulations.

D. Performance of the DCPC Probe with a Realistic Detector

As it was described in section II.A, the spatial resolution of each layer of the detector is a crucial parameter for the characterization of the probe performance. In order to assess these parameters, the simulation of optical photons was added to the GATE model used in the previous section. The physical and scintillation properties of the EJ-200 plastic scintillator (ELJEN Technology, Texas, USA) were used for each layer: scintillation yield of 1×10^4 photons/MeV, refractive index of 1.58 and an emission spectrum with the wavelength of maximum emission at 425 nm. For the photon sensor, a SiPM that covers the whole area of the plastic scintillator was positioned on the external face of the back layer (see Fig. 3). The SiPM sensitive photo-cathode was coupled to the back layer in two different ways: in direct contact and with a 2 mm thick light guide to spread the light and allow the possibility of interpolating between detector pixels. All the transition surfaces were defined as *smooth* (polished). The refractive index of the glass was 1.5.

A collimated $^{18}\mathrm{F}$ point source was simulated for each of the configurations of interest. The simulations were processed by integrating the optical photons arriving to the SiPM over a time window of 1 μs. Next, the SiPM photon detection efficiency (PDE) was accounted for by simulating a random process where each photon arriving to the SiPM was accepted or rejected using detection probabilities of 0.25, 0.5 and 1 (PDE values of 25%, 50% and 100%). Then, the optical photons that were detected by the SiPM were split into two groups, one for those originating in the front layer and another for the back layer. The centroid of the optical photons in each of group was used to estimate the impact point on each layer using SiPM granularities of 0.1, 0.5 and 1 mm. The spatial resolution in FWHM was computed for each layer. Histograms of the number of optical photons for each layer, as well as of their spatial distribution on the SiPM, were also recorded.

Finally, a complete assessment of the probe was performed by placing a $^{18}\mathrm{F}$ point source at 10 mm from the probe. The events were processed in the same way as described previously in this section. The LORs needed for the image reconstruction were generated using the (x, y) centroid and the coordinate of the centre of the scintilator in z, for each layer.

E. Image Reconstruction

The images were reconstructed by backprojecting the LORs into the imaging plane to assess the intrinsic resolution of the system. However, statistical methods that model the noise of the data and the acquisition process can improve the image quality in terms of resolution and noise as has been shown for PET imaging [20]. The emission of positrons from a radiotracer follow a Poisson distribution and, as a consequence, the positron counts detected in the probe can be considered as Poisson random variables. The log-likelihood function for Poisson data m with mean value q is given by:

$$\ln l(m|f) = \sum_{i=1}^{I} m_i \ln(q_i(f)) - q_i(f) - \ln(m_i!) \qquad (8)$$

where f is the radiotracer distribution, m is a vector with the measured data and q is the modelled mean value for the data using a linear model:

$$q_i = \sum_j^J a_{ij} f_j \tag{9}$$

where a_{ij} is an element (i, j) of the system matrix A and gives the probability that a positron emitted in pixel j is detected in LOR i.

The maximum likelihood (ML) for Poisson data is obtained by maximizing equation 8. For the proposed system, where the reconstruction is done into an imaging plane and the data are stored in list-mode, the ML estimator corresponds to the case of complete data because every LOR is backprojected into only one pixel for the case of nearest neighbour interpolation. In this case, the reconstructed image is given by:

$$f_j = \frac{\sum_{l \in L_j} 1}{\sum_i^I a_{ij}} \tag{10}$$

where f_j is the pixel j of the reconstructed image, the numerator is the sum over the set L_j of all detected events that are backprojected into pixel j. The denominator is the pixel j of the sensitivity image computed by backprojecting all the I possible LORs in the system.

When the resolution of the system is modelled in the system matrix, an LORs is backprojected into several pixels. Therefore now the data are incomplete and a closed-form solution is not available for the ML estimate. As for PET reconstruction, we can use the iterative MLEM algorithm [21], [22] to get the ML reconstructed image. The MLEM algorithm for list-mode data is defined by:

$$f_j^{n+1} = \frac{f_j^n}{\sum_{i=1}^I a_{ij}} \sum_{l=1}^L a_{lj} \frac{1}{\sum_{k=1}^K a_{lk} f_k^n} \tag{11}$$

where f_j^n is the pixel value of the reconstructed image at index j and iteration number n, l is the index in the list of the L acquired events, i is the index for the set of all I possible LORs in the system and the other parameters are the same as for the previous equations.

We reconstructed the simulated data obtaining the ML estimate of complete data (without resolution modelling) and also using the MLEM algorithm when modelling the resolution of the system. The model for the system matrix included the detection solid angle:

$$a_{ij} = w_{ij} (\frac{1}{d_{ij}})^2 \tag{12}$$

where w_{ij} is the geometrical probability that an event detected in LOR i was emitted in pixel j and d_{ij} is the distance between the position of the LOR i in the back layer and the coordinates of pixel j. When no resolution modelling is applied, w_{ij} is 1 only for one pixel per LOR; when the resolution is modelled, w_{ij} is a Gaussian kernel centred at the backprojected coordinates.

To model the resolution in the reconstruction, we used a Gaussian kernel obtained from the backprojected images of a point source. Because each simulated configuration has a different spatial resolution, a different kernel was used for each configuration. In addition to the point source, a phantom with four point sources was used to evaluate the reconstructed images. The sources were placed at (0,0) mm, (15,15) mm, (-10,15) mm and (-20,-20) mm.

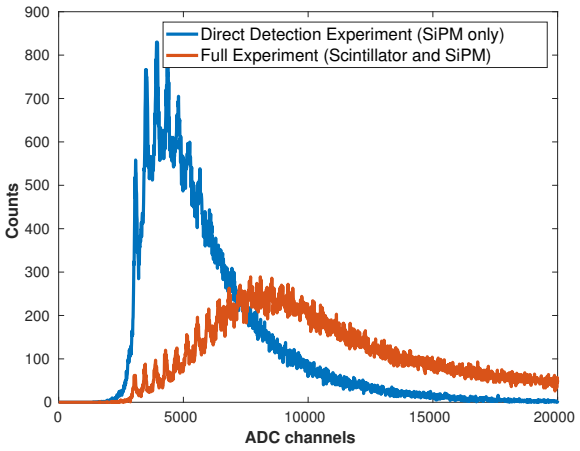

Fig. 6. Energy spectrums, in units of ADC channels, for two experimental setups: a ^{90}Sr disc source measured with only a SiPM to assess direct detection of positrons; and the same source measured with the full detector, that consisted of a 25 µm plastic scintillator and the SiPM. The peaks correspond to a specific number of triggered cells, which can be resolved so long as the peak width is smaller than the peak-to-peak distance, and the width increases with the squared root of the number of cells.

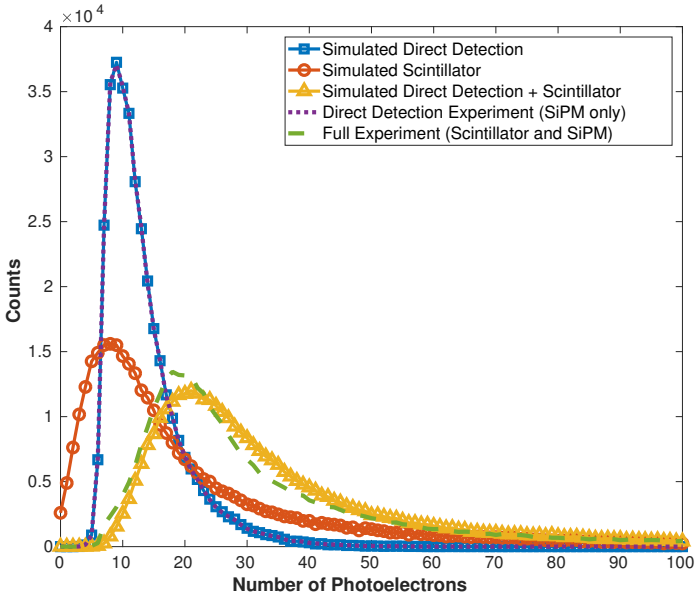

Fig. 7. Number of photoelectrons for simulated and experimental measurements of a ^{90}Sr disc source with a 25 µm plastic scintillator and a SiPM. The number of photoelectrons coming from direct detection in the SiPM, from the scintillator and the sum of both quantities are shown for the simulated data; while the number of photoelectrons for the experimental data are shown for setups with the point source and the SiPM (direct detection), and for the point source with the scintillator and SiPM (sum of photons from direct detection and scintillator)

F. Measurement Validation

A simple experiment using only one detection layer was used to validate the Monte Carlo simulations used in this work. The experiment consisted of the measurement of the signal spectrum of a ^{90}Sr disc source located on the surface of a detector made of a plastic scintillator and a single SiPM. The plastic scintillator used was the EJ-214 by Eljen Techonolgy, with an area of 10×10 mm^2, a thickness of 25 µm and a density of 1.02 g cm^{-3}. The SiPM has a photodetection efficiency of 25%, an area of 6x6 mm^2, with 50 µm cell size and a dark count rate of $\sim$10 mHz for a 5 photo-electron

threshold. The same configuration was modelled and simulated with GATE. The SiPM efficiency was taken into account as well as the photo-electron threshold in the readout.

In order to compare simulation and experiment, the effect due to the direct detection of ionising particles in the sensor had to be taken into account. In fact, because of the extremely low thickness of the scintillator, the majority of the particles emitted by the source enter the sensitive volume of the SiPM, generating charge carriers which trigger avalanches in the SiPM. In order to model the effect, details about the junction design and technology, the electric field profile and the material are required. As these sensors are commercial products, these details are not disclosed by the manufacturer and a different approach was followed. The experimental spectrum from the direct detection was convolved with the simulated spectrum due to the scintillating light and compared to the experimental data.

The energy spectrum due to the direct detection in the SiPM was obtained by positioning the ^{90}Sr disc source directly on the SiPM surface. In Fig. 6, the energy spectrum for direct detection is shown, where the peaks corresponding to the different number of fired cells can be distinguished. Using the peak-to-peak value, the spectrum can be converted into the probability density function (PDF) of photoelectrons for direct detection (dotted line in Fig. 7). Using this PDF and its respective cumulative distribution function (CDF), the Monte Carlo simulation was complemented with the number of photoelectrons that would be generated by direct detection in the SiPM. For every detected event in the Monte Carlo simulation, a random number between 0 and 1 was generated and used as input in the CDF in order to obtain the number of photoelectrons generated by direct detection for that event in the simulated signal.

In Fig. 7, a histogram of the number of photoelectrons is shown for the Monte Carlo simulation that takes into account only the photoelectrons generated by the scintillator (full line with circle markers), for the simulated direct detection (full line with square markers) and for the sum of both signals (full line with triangle markers). The latter would be equivalent to the signal obtained in the experimental setup when measuring the point source with the scintillator, which is shown in the figure with a dashed line. The simulated and experimental distribution of photoelectrons have a very good agreement in terms of shape and most probable value, showing that the models used in the simulations used to assess the DCPD concept are an accurate representation of real data, even for configurations with ultra thin scintillators where a small number of optical photons are generated. The simulated histogram of the number of photoelectrons for direct detection matches perfectly the experimental histogram because the number of photons due to direct detection was simulated using a CDF obtained from the experimental data and therefore they are expected to exactly overlap for a large number of simulated events.

III. Results and Discussion

A. Essential Features of the DCPD Probe under Realistic Working Conditions

Fig. 8 shows the count rates as a function of the scintillator thickness for the simulation of a hot lesion within a body phantom that emits a gamma background. The coincidence events and single events in each detection layer are shown separately for the particles coming from the hot source and from the background. It can be

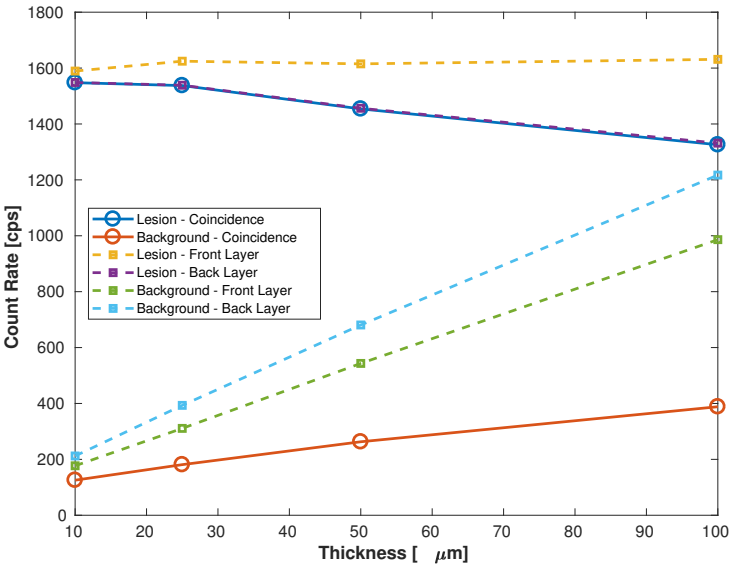

Fig. 8. Count rates as a function of the scintillator thickness for the simulation of a hot lesion embedded at 0.1 mm from the surface with a background source uniformly distributed in the patient's body. The coincidence event rates and single event rates per detection layer are shown separately for the events coming from the hot source and from the background.

observed that the background has low impact for the coincidence events, being only 10% of the tumour coincidence rate for a layer thickness of 10 µm. With thicker layers, the gamma background rejection worsens as the detectors are more sensitive to gamma radiation. However, for thick layers of 100 µm the coincidence rate for the background is only 25% of the tumour coincidence rate despite the fact that the rates for single events are much closer. It is worth noting that the background coincidences are mainly due to the detection in both layers of the same photon or positron that was emitted by the background source, and not due to random coincidences between the two layers. Moreover, the counts of the source are spatially localized while the background is uniformly distributed and, as a consequence, the impact of the background is even less considerable as can be seen in the profile of the backprojected image for the simulation with 100 µm thickness scintillators (Fig. 9). This shows the effectiveness of using a dual layer probe to improve the gamma background rejection (when a good layer discrimination is available) due to the low sensitivity of thin scintillators to gamma photons.

In agreement with section II-B, Fig. 8 shows that the front layer is more sensitive to the radiation coming from the lesion than the back layer. On contrary, for the background source the back layer is more sensitive than the front layer since the simulated probe has no shielding and, due to the large size of the background source, the solid angle seen by the back layer is larger for a point source located in the outer regions of the volumetric source.

On account of the negligible impact of the gamma background on the backprojected images, the background source was not included in the simulations used to assess the spatial resolution as a function of the scintillator thickness and of the air gap between them. Fig. 10 shows profiles of the backprojected images for the simulation of a point source at 10 mm from the probe, with and without the foil cover, for scintillator thicknessess of 10, 25, 50 and 100 µm and an air gap of 150 µm. The profiles have very low noise

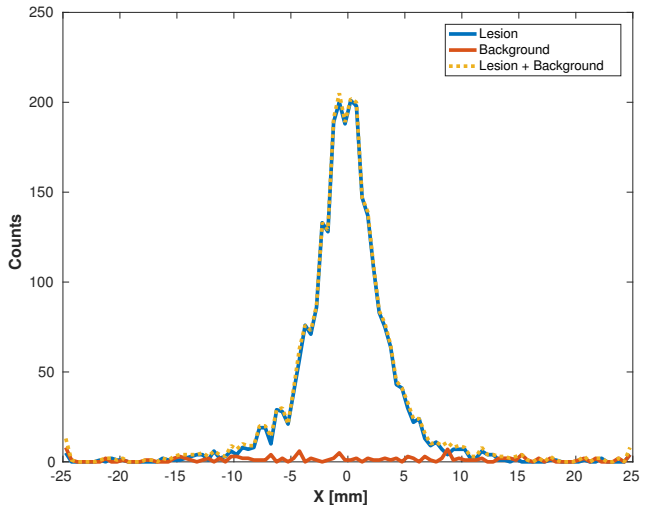

Fig. 9. Profiles of the backprojected image for the simulation of the probe with a scintillator thickness of 100 μm scanning a hot lesion with a background source uniformly distributed in the patient's body.

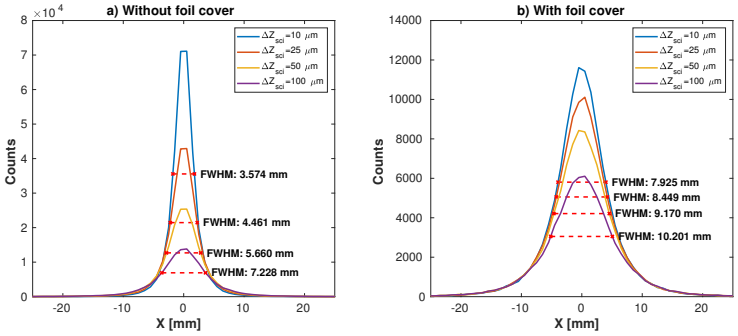

Fig. 10. Profiles of the backprojected images for a long scan of a point source scan for scintillator thicknessess of 10, 25, 50 and 100 μm and an air gap of 150 μm. a) Without the foil cover. b) With the foil cover.

since a long scan of 20 min was simulated. We can observe the high impact that the introduction of a foil cover has on the spatial resolution of the system. For these simulations, the other values of separation between layers were not presented since they gave similar values to a separation distance of 150 μm. This agrees with the theory previously developed, where the distance between layers has negligible impact when an ideal detector (perfect estimation of the impact point) is simulated and therefore the degradation of the spatial resolution depends only on the deviation of the positrons in the front layer. In this subsection we used the backprojected images to characterize the intrinsic spatial resolution of the system, but iterative reconstruction methods can improve the spatial resolution of the reconstructed images. To summarize, Fig. 11 shows the FWHM as a function of the scintillator thickness for the simulated probe with and without the foil cover.

B. Performance of the DCPC Probe with a Realistic Detector

Fig. 12 shows the spatial resolution in FWHM of the simulated realistic detector for each layer and the mean number of detected optical photons for different probe configurations. A SiPM with a pixel size of 0.1 mm was simulated. The plots in red are for a PDE of 100%, in blue for 50% and in magenta for 25%. As expected a thicker scintillator has a better spatial resolution thanks to the

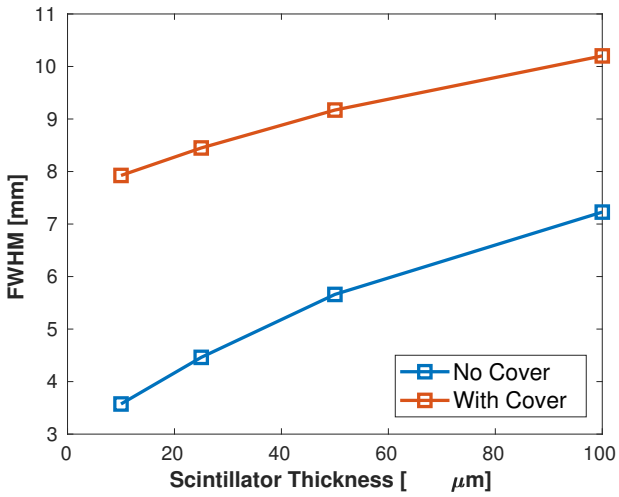

Fig. 11. FWHM of the backprojected images as a function of the scintillator thickness for the simulation of a point source at 10 mm from the probe, with and without the foil cover and taking into account only the positron physics.

generation of a larger amount of optical photons. The front layer has a lower spatial resolution because fewer photons coming from this layer arrive to the SiPM. The latter depends on the air gap between layers, where a larger gap results in fewer photons and as a consequence a poorer spatial resolution. For a PDE of 25%, the number of detected optical photons coming from the front layer was extremely low, not only adversely affecting the resolution but also the sensitivity, such that several events had no photons from the front layer detected. For this reason, we did not use this efficiency value in the general assessment of the probe.

It can also be seen that when a 2 mm thick light guide is included, the effect is contrary to what was originally intended. Instead of being able to interpolate between pixels to obtain a more accurate centroid, the centroid had a much larger error due to the reduced number of photons, especially from the front layer. In Fig. 13, a 2D histogram with the spatial distribution of optical photons for each layer is shown for each configuration. These histograms show the distribution of optical photons after detecting 1×10^4 positrons. For the back layer with a light guide, a different spatial distribution pattern is observed, this could be due to the reflection of photons on the interface between the back layer scintillator and the air gap.

For detector pixel sizes of 0.5 and 1 mm and a configuration without a light guide, similar results were obtained to the 0.1 mm pixel size except for a slight resolution degradation on the front layer. This has to do with the fact that the spread of the light is very narrow in these configurations and therefore the uncertainty due to the number of optical photons has less impact (most of the optical photons are concentrated on a few detector pixels). In addition, with a granularity of 0.1 mm the minimum achievable resolution is 0.3 mm, therefore increasing the granularity to 0.5 mm has little impact on the spatial resolution.

In summary, the best detector configuration in terms of spatial resolution of the impact points on each layer is a 100 μm scintillator thickness and a 150 μm air gap, where resolutions of 0.35 and 0.25 mm FWHM were obtained for the front and back layer respectively for a PDE of 100%. However, this does not mean that this is the best configuration for the estimation of the emission point, since a

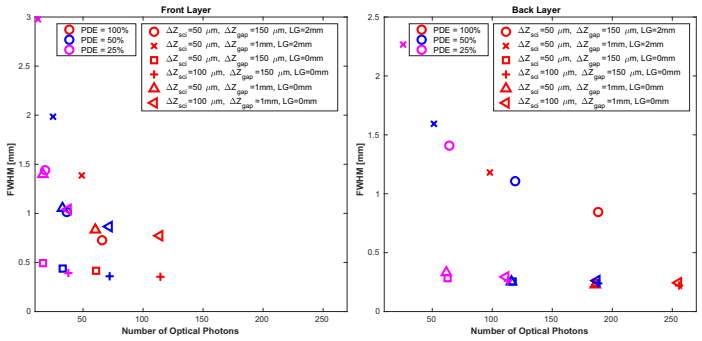

Fig. 12. Spatial resolution of the detector as function of the number of optical photons for detectors with a light guide (LG) of 2 mm (circle and x-mark) and without light guide for probe configurations with layer thicknesses of 50 and 100 µm, air gap of 150 µm and 1 mm and SiPM with 0.1 mm pixel pitch. Results for 100% PDE are shown in red and for 50% PDE in blue.

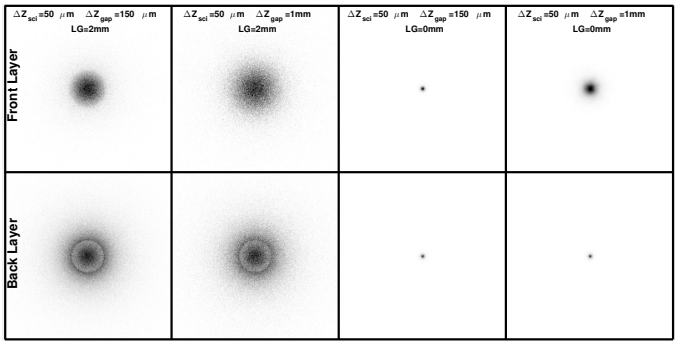

Fig. 13. Spatial distribution of optical photons on the SiPM surface obtained after the impact of 1×10^4 positrons for different probe configurations.

thicker scintillator means a larger deviation of the positron in each layer and a smaller air gap results in a larger amplification of the error of the impact points when the LOR is backprojected. The error in the backprojected LOR can be analysed using equation (3) and, when taking into account this factor, the configuration with a 100 µm scintillator thickness and a 1 mm air gap is the best option with a resolution in the backprojected point of 8 mm FWHM.

In the final assessment of the probe, the sensitivity and the resolution of the reconstructed emission points are the main parameters of interest. In Fig. 14 the overall results for the simulations that take into account the optical photons are shown. The results refer to a SiPM with 100% PDE. Fig. 14-a shows the FWHM of the backprojected images as a function of the scintillator thickness for a point source at 10 mm from the probe, for probes with an air gap of 150 µm and 1000 µm and a SiPM with pixel pitch of 0.1, 0.5 and 1 mm. For an air gap of 150 µm the spatial resolution of the backprojected images is affected by the readout granularity (in particular for the 1 mm pixel pitch) due to the amplification by a factor of n of the detector spatial resolution as described in equation (7). On the contrary, for the case of a 1000 µm air gap the three pitch values gave similar FWHM values, showing that increasing the air gap is a good strategy to reduce the image resolution loss due to the readout limited spatial resolution. The disadvantage of a larger air gap is a decrease in the probe sensitivity, which was a 10% reduction for a 1000 µm air gap (compared to a 150 µm gap) as shown in Fig. 14-b, due to a smaller acceptance angle for coincidence events. Importantly, when optical photons are taken into account, thinner layers obtained larger FWHM values due to the low number of photons generated by thinner scintillators, resulting in a larger error on the estimation of the centroid of the detected photon positions. In Fig. 14-a, a scintillator thickness of 50 µm showed the best performance in terms of spatial resolution without having a big loss of sensitivity. A thickness of 25 µm also proved to be a good compromise solution, achieving the best sensitivity and a comparable spatial resolution to the probe with a 50 µm scintillator thickness.

In Fig. 14-a the spatial resolution that would be obtained with a ideal detector is represented by dashed lines with triangular markers. For a 100 µm scintillator thickness and a 1000 µm gap, the resolution goes from 8 mm to approximately 11 mm when including the generation and detection of optical photons. These results match what could be predicted using equation (7), where the term due to the positron deviation would be the resolution with a perfect detector (8 mm FWHM for the case being analysed) and the terms due to the spatial resolution of the detector can be obtained from the previous section (also approximately 8 mm FWHM); giving a total predicted resolution of 11.3 mm FWHM that is similar to the resolution values observed in Fig. 14-a.

A critical issue in the reconstruction of the particle trajectory is the significant reduction in the number of detected photons arriving from the top layer as was shown in the previous section. Fig. 15 shows the number of detected optical photons generated in the front (a) and back (b) layers. The reason why most of the photons of the first layer do not arrive to the SiPM is the interface between the scintillator and the air gap, where a transition from a material with larger refractive index (plastic scintillator) to a material with lower refractive index (air) occurs (see Fig. 3). The critical angle from which photons start to be reflected can be computed using Snell's law with the refractive indices of air and the simulated plastic scintillator. The critical angle for the interface in the front layer is approximately 40° and therefore a considerable number of the optical photons emitted in the front layer are reflected and do not arrive at the SiPM.

In this set of simulated experiments, the possibility of using different thicknesses for the front and back layers has not been explored. However, it has been shown that the key parameter limiting the performance of the probe is the thickness of the front layer and this parameter was optimized to achieve the better overall performance. A thicker layer could be used in the back layer in order to improve the spatial resolution of the estimated impact point, but it is expected to bring little benefit since the spatial resolution of the impact point on the front layer and the deviation of the particle in the foil cover and the front layer are the dominating factors that limit spatial resolution.

C. Image Reconstruction

The ML reconstruction of the simulated data for a point source and for the phantom with multiple sources is shown in Fig. 16. The simulated experiments consisted of a 1 min scan for each phantom and they included the simulation of optical photons and the SiPM readout. The probe had a scintillator thickness of 25 µm, an air gap of 1000 µm and the foil cover was not included. The ML reconstructions without resolution modelling (complete data)

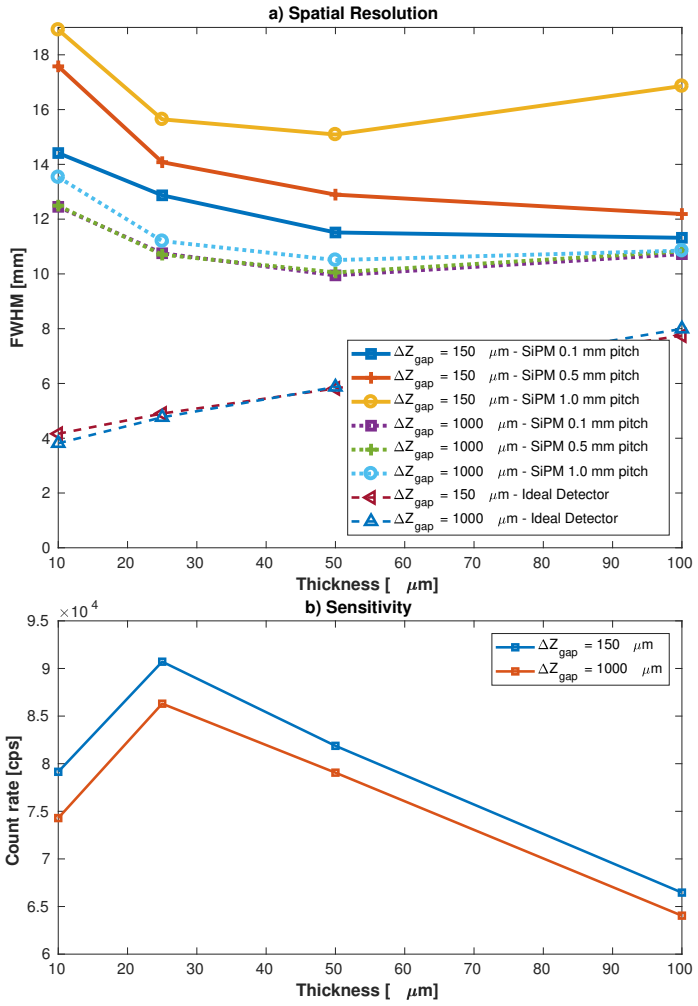

Fig. 14. Results for the simulations of a point source at 10 mm from the probe taking into account the optical photons generation and the SiPM readout, for probes with an air gap of 150 µm and 1000 µm and a SiPM with pixel pitch of 0.1, 0.5 and 1 mm. a) Spatial resolution in the backprojected images as a function of the scintillator thickness. b) Sensitivity as a function of the scintillator thickness and the air gap. The trade-off between spatial resolution and sensitivity can be observed.

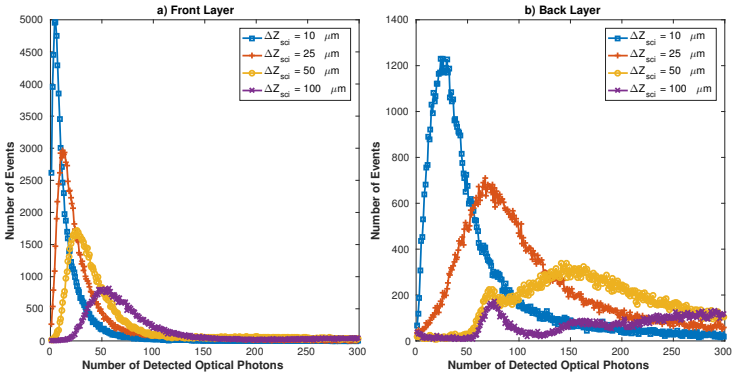

Fig. 15. a) Number of optical photons detected by the SiPM coming from the front layer for scintillator thicknessess of 10, 25, 50 and 100 µm. b) Number of optical photons detected by the SiPM coming from the back layer for scintillator thicknessess of 10, 25, 50 and 100 µm.

are shown along with the MLEM reconstruction with resolution modelling. There is a large improvement in the final resolution when the resolution model is included. In Fig. 17 the resolution

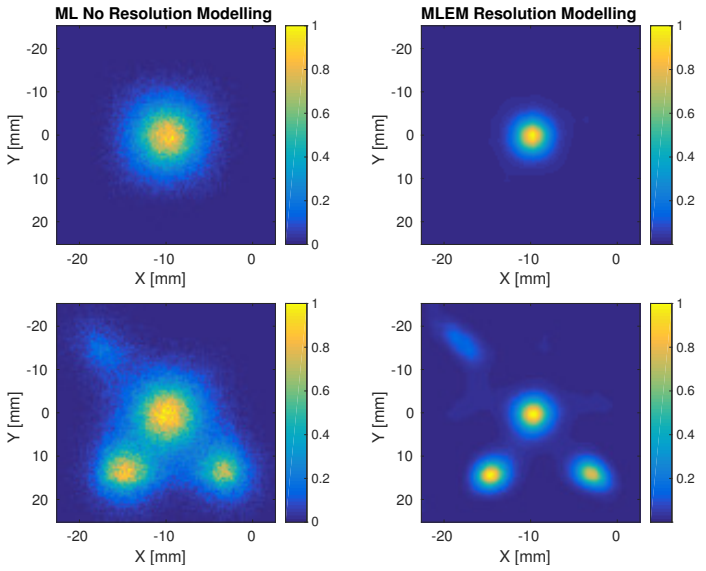

Fig. 16. Reconstructed images with ML without resolution modelling (left) and MLEM with resolution modelling (right) with 100 iterations, for a point source (top) and multiple point sources (bottom).

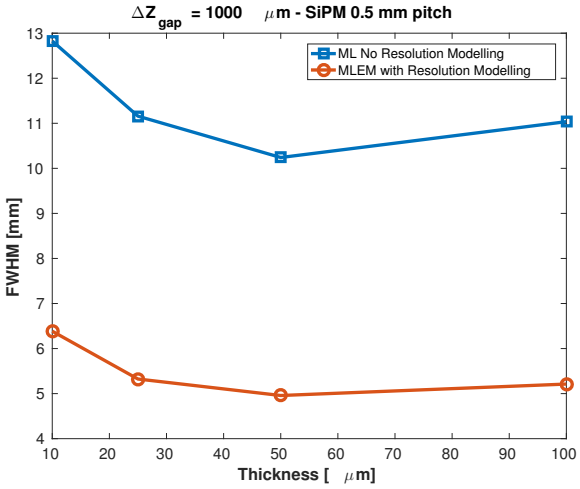

Fig. 17. FWHM as a function of the scintillator thickness for the reconstruction of a point source with ML without resolution modelling and MLEM with resolution modelling. The simulation included the optical photons and SiPM readout, and the air gap in the probe was 1000 µm.

improvement with the MLEM reconstruction algorithm was quantified by computing the FWHM of the reconstructed point source as a function of the scintillator thickness for an air gap of 1000 µm. The resolution was improved by a factor of ~ 2 reduction of the FWHM compared to the backprojected images.

IV. Conclusions

The design of an intra-operative probe based on the DCPD concept has several challenges to be addressed. The physics of positron detection imposes a limit on the resolution that this type of device can achieve. For a working distance of 10 mm, the intrinsic resolution of the system is 4.5-5.5 mm FWHM for a scintillator thickness of 25-50 µm. A thinner scintillator cannot be used due to the reduced number of optical photons that would be generated. In addition, a cover is needed to protect the front layer of the probe,

which degrades the intrinsic practical resolution by about 70% to 8-9 mm. When we take into account the detection of the optical photons and the readout of the photo-detector, the best resolution was achieved for scintillator thicknesses of 50 $\mu\mathrm{m}$. However, with a thickness of 25 $\mu\mathrm{m}$ a spatial resolution almost as good can be achieved and with a higher sensitivity. An important reason for the poor spatial resolution of the system is the large errors in the estimation of the positron interaction position in the front layer, as a result of the limited number of optical photons arriving at the SiPM due to reflections that occur in the scintillator-air interface of the front layer.

The use of the MLEM image reconstruction algorithm with resolution modelling can considerably improve the resolution of the reconstructed images. For the simulation of the probe taking into account a realistic detector but without including the foil cover, a point source reconstructed with a simple backprojection achieves a FWHM of $\sim 10\ \mathrm{mm}$, while with the MLEM algorithm the resolution is improved to $\sim 5\ \mathrm{mm}$.

The simulation study presented in this work shows that the use of a DCPD is a good design for an imaging probe that considerably improves the positron-gamma discrimination compared to single layer and gamma probes. However, the use of a DCPD detector cannot achieve the resolution ideally needed to assist surgeons with tumour removal. This limitation can be partially compensated for by using statistical reconstruction algorithms that can improve the resolution closer to the requirement of 5 mm. An additional problem, is the need of a foil cover to avoid contact with the tissue and contamination, which degrades the resolution by at least $\sim 3\ \mathrm{mm}$ FWHM (60% degradation for the case of an ideal detector with scintillator thicknessess of 50 $\mu\mathrm{m}$).

To conclude, according to our study an imaging intra-operative probe using DCPD is not yet feasible due to the low spatial resolution obtained with current technology. Nevertheless, the reduction of the thickness of the foil cover, the introduction of new plastic scintillators with better light yields and lower refractive indices along with current advances in SiPMs (i.e. higher efficiency and smaller pixel sizes) are key factors that could change the situation and result in spatial resolutions closer to that required for an intra-operative probe.

V. Acknowledgments

This work was supported by Innovate UK [101682]; the Engineering and Physical Sciences Research Council [EP/M020142/1]; and by the Wellcome/EPSRC Centre for Medical Engineering [WT 203148/Z/16/Z].

References

[1] R. Jeevan, D. A. Cromwell, M. Trivella, G. Lawrence, O. Kearins, J. Pereira, C. Sheppard, C. M. Caddy, and J. H. P. van der Meulen, "Reoperation rates after breast conserving surgery for breast cancer among women in England: retrospective study of hospital episode statistics," *BMJ*, vol. 345, p. e4505, 2012.

[2] F. Daghighian, J. C. Mazziotta, E. J. Hoffman, P. Shenderov, B. Eshaghian, S. Siegel, and M. E. Phelps, "Intraoperative beta probe: A device for detecting tissue labeled with positron or electron emitting isotopes during surgery," *Med. Phys.*, vol. 21, no. 1, pp. 153–157, jan 1994.

[3] C. S. Levin, L. R. Macdonald, M. P. Tornai, E. J. Hoffman, and J. Park, "Optimizing light collection from thin scintillators used in a beta-ray camera for surgical use," *IEEE Trans. Nucl. Sci.*, vol. 43, no. 3, 1996.

[4] E. J. Hoffman, M. P. Tornai, C. S. Levin, L. R. MacDonald, and C. H. Holdsworth, "A dual detector beta-ray imaging probe with gamma-ray background suppression for use in intra-operative detection of radiolabeled tumors," *Nucl. Instr. Meth. Phys. Res. A*, vol. 409, no. 1-3, pp. 511–516, 1998.

[5] R. R. Raylman, "Performance of a dual, solid-state intraoperative probe system with 18F, 99mTc, and (111)In." *J. Nucl. Med.*, vol. 42, no. 2, pp. 352–360, 2001.

[6] M. Piert, M. Burian, G. Meisetschläger, H. J. Stein, S. Ziegler, J. Nährig, M. Picchio, A. Buck, J. R. Siewert, and M. Schwaiger, "Positron detection for the intraoperative localisation of cancer deposits," *Eur. J. Nucl. Med. Mol. Imag.*, vol. 34, no. 10, pp. 1534–1544, sep 2007.

[7] H. Sabet, B. C. Stack, and V. V. Nagarkar, "A Hand-Held, Intra-Operative Positron Imaging Probe for Surgical Applications," *IEEE Trans. Nucl. Sci.*, vol. 62, no. 5, pp. 1927–1934, 2015.

[8] A. Russomando, F. Bellini, V. Bocci, F. Collamati, E. D. Lucia, R. Faccini, M. Marafini, I. Mattei, G. Chiodi, V. Patera, L. Recchia, A. Sarti, A. Sciubba, E. S. Camillocci, R. Paramatti, C. Voena, R. Donnarumma, C. Mancini-Terracciano, and S. Morganti, "An intraoperative $beta^-$ detecting probe for radio-guided surgery in tumour resection," *IEEE Trans. Nucl. Sci.*, vol. 63, no. 5, pp. 2533–2539, Oct 2016.

[9] R. Essner, E. C. Hsueh, P. I. Haigh, E. C. Glass, Y. Huynh, and F. Daghighian, "Application of an [18F]Fluorodeoxyglucose-Sensitive Probe for the Intraoperative Detection of Malignancy," *J. Surg. Res.*, vol. 96, no. 1, pp. 120–126, 2001.

[10] B. Meller, K. Sommer, J. Gerl, K. von Hof, A. Surowiec, E. Richter, B. Wollenberg, and M. Baehre, "High energy probe for detecting lymph node metastases with 18F-FDG in patients with head and neck cancer." *Nuklearmedizin*, vol. 45, no. 4, pp. 153–9, 2006.

[11] S. A. Gulec, F. Daghighian, and R. Essner, "PET-Probe: Evaluation of Technical Performance and Clinical Utility of a Handheld High-Energy Gamma Probe in Oncologic Surgery," *Ann. Surg. Oncol.*, vol. 23, no. S5, pp. 9020–9027, dec 2016.

[12] V. E. Strong, C. J. Galanis, C. C. Riedl, V. A. Longo, F. Daghighian, J. L. Humm, S. M. Larson, and Y. Fong, "Portable PET probes are a novel tool for intraoperative localization of tumor deposits." *Ann. Surg. Innov. Res.*, vol. 3, p. 2, feb 2009.

[13] L. Chen, L. S. Gobar, N. G. Knowles, D. W. Wilson, and H. H. Barrett, "Direct Charged-Particle Imaging System Using an Ultra-Thin Phosphor: Physical Characterization and Dynamic Applications," *IEEE Trans. Nucl. Sci.*, vol. 56, no. 5, pp. 2628–2635, 2009.

[14] E. J. Hoffman, M. P. Tornai, C. S. Levin, L. R. MacDonald, and S. Siegel, "Gamma and beta intra-operative imaging probes," *Nucl. Instr. Meth. Phys. Res. A*, vol. 392, no. 1-3, pp. 324–329, 1997.

[15] S. C. Thacker, B. C. Stack, V. Lowe, V. Gaysinskiy, S. Cool, V. V. Nagarkar, and G. Entine, "A novel imaging beta probe for radio-guided surgery," in *2008 IEEE NSS/MIC Conference Record*. IEEE, oct 2008, pp. 3875–3878.

[16] H. H. Barrett, B. Miller, Y. Ding, L. Chen, J. W. Hoppin, and L. Caucci, "Beta and Alpha Emission Tomography for Three-Dimensional Autoradiography," *International patent application (PCT/US15/14223)*, 2014.

[17] Y. Ding, L. Caucci, and H. H. Barrett, "Directional charged-particle detector with a two-layer ultrathin phosphor foil," in *2014 IEEE NSS/MIC Conference Record*. IEEE, nov 2014, pp. 1–4.

[18] J. Hubbell and S. Seltzer, "Tables of X-Ray Mass Attenuation Coefficients and Mass Energy-Absorption Coefficients (version 1.4)," 2004. [Online]. Available: http://physics.nist.gov/xaamdi

[19] S. Jan, G. Santin, D. Strul, S. Staelens, K. Assié, D. Autret, S. Avner, R. Barbier, M. Bardiès, P. M. Bloomfield, D. Brasse, V. Breton, P. Bruyndonckx, I. Buvat, A. F. Chatziioannou, Y. Choi, Y. H. Chung, C. Comtat, D. Donnarieix, L. Ferrer, S. J. Glick, C. J. Groiselle, D. Guez, P.-F. Honore, S. Kerhoas-Cavata, A. S. Kirov, V. Kohli, M. Koole, M. Krieguer, D. J. van der Laan, F. Lamare, G. Largeron, C. Lartizien, D. Lazaro, M. C. Maas, L. Maigne, F. Mayet, F. Melot, C. Merheb, E. Pennacchio, J. Perez, U. Pietrzyk, F. R. Rannou, M. Rey, D. R. Schaart, C. R. Schmidtlein, L. Simon, T. Y. Song, J.-M. Vieira, D. Visvikis, R. V. de Walle, E. Wieërs, and C. Morel, "GATE: a simulation toolkit for PET and SPECT," *Phys. Med. Biol*, vol. 49, no. 19, pp. 4543–4561, oct 2004.

[20] R. Leahy and J. Qi, "Statistical approaches in quantitative positron emission tomography," *Stat. Comput.*, vol. 10, no. 2, pp. 147–165, jan 2000.

[21] K. Lange and R. Carson, "EM reconstruction algorithms for emission and transmission tomography." *J Comput Assist Tomogr*, vol. 8, no. 2, pp. 306–16, apr 1984.

[22] L. A. Shepp and Y. Vardi, "Maximum Likelihood Reconstruction for Emission Tomography," *IEEE Trans. Med. Imag.*, vol. 1, no. 2, pp. 113–122, 1982.